


3D-Mössbauer spectroscopic microscope for mc-Si solar cell evaluation

Y. Ino¹  · H. Soejima¹ · K. Hayakawa¹ · K. Yukihiro¹ ·
K. Tanaka¹ · H. Fujita¹ · T. Watanabe¹ · K. Ogai² ·
K. Moriguchi² · Y. Harada² · Y. Yoshida¹

© Springer International Publishing Switzerland 2016

Abstract A 3D-Mössbauer Spectroscopic Microscope is developed to evaluate Fe impurities in multi-crystalline Si solar cells, which combines the Mössbauer spectroscopic microscope with a scanning electron microscope (SEM), an electron beam induced current (EBIC), an electron backscatter diffraction (EBSD), and an electron energy analyzer (HV-CSA). In addition, a new moving-coil-actuator with a linear encoder of 100 nm-resolution is incorporated for the operations with both a constant velocity and a constant acceleration mode successfully with the same precision as that obtained by the conventional transducers. Furthermore, a new multi-capillary X-ray lens is designed to achieve a γ -ray spot size less than 100 μm in diameter. The new microscope provides us to investigate the space correlation between Fe impurities and the lattice defects such as grain boundaries in multi-crystalline Si solar cells.

Keywords ^{57}Fe Mössbauer spectroscopy · Mapping · Imaging · MCX · Si solar cells

1 Introduction

We have built a new “3D-Mössbauer Spectroscopic Microscope (MSM)” to evaluate multi-crystalline (mc-) Si solar cells [1, 2], which contain Fe impurities incorporated during

This article is part of the Topical Collection on *Proceedings of the International Conference on the Applications of the Mössbauer Effect (ICAME 2015), Hamburg, Germany, 13–18 September 2015*

✉ Y. Ino
y-ino@ob.sist.ac.jp

¹ Shizuoka Institute of Science and Technology, 437-8555, Toyosawa 2200-2, Fukuroi, Shizuoka, Japan

² APCO. Ltd., 192-0906, Kitano-cho 522-10, Hachioji, Tokyo, Japan

production processes, leading to a serious degradation in the energy conversion efficiency. Fe impurities in mc-Si are considered to possess different charge states on different lattice sites, yielding different carrier-trapping cross-sections [3]. The Fe impurities are expected to distribute on different lattice sites under the influence of grains and defects in mc-Si solar cells [4]. So far, no evaluation technique has been reported which enables to provide such atomistic information simultaneously even under the solar cell operation.

In order to investigate the interactions and the correlations between Fe impurities and the lattice defects such as dislocations, grain boundaries, and residual strains in different grains, we have combined our new MSM system with a scanning electron microscope (SEM), an electron beam induced current (EBIC), an electron backscatter diffraction (EBSD), and an optical microscope. In addition, we are trying to get a 3D-mapping image by a cylindrical sector electron analyzer (HV-CSA), which measures the energy dissipation of conversion and Auger electrons emitted from Fe impurities in solar cells. In this paper, we report on the set-up and the characteristics of the new MSM system.

2 Experimental system

Figure 1 shows the three dimension (3D-) Mössbauer spectroscopic microscope (MSM) and its horizontal cross section. The MSM system consists of a moving-coil linear-actuator coupled with a linear encoder (LAL20-025-52M, SMAC) as a Mössbauer driver, a multi-capillary X-ray lens (MCX, Hamamatsu Photonics) to focus the 14.4 keV γ -rays, a Si-PIN γ -rays detector (XR-100CR, AMPTEK), a new three-stage micro-channel-plate (MCP, Hamamatsu Photonics) with a funnel structure to detect the conversion and Auger electrons due to the Mössbauer effect, an X-Y-Z precision stage (Kohzu Precision) mounted on a vacuum chamber, and a LIST-mode data acquisition system (A3400, NIKI GLASS).

In order to investigate iron impurities in mc-Si solar cells by MSM in association with the lattice defects, grains, and residual stresses, SEM (MINI-EOC, APCO), EBIC, and EBSD (QUANTAX, Bruker) are also installed, so that all the measurements can be carried out in the same area by rotating a sample holder. To obtain 3D images of Fe distribution, a cylindrical sector electron analyzer (HV-CSA, FOCUS) is incorporated to measure the energy dissipations of conversion and Auger electrons which are emitted from ^{57}Fe nucleus after the recoil-free 14.4 keV γ -ray absorption (Mössbauer effect), and subsequently are escaping from a solid. To suppress the vibration of a sample, the entire system is mounted on a vibration isolation table (KURASHIKI KAKO).

3 Results and discussion

Figure 2 shows the performance of a moving-coil actuator coupled with a 100nm-resolution linear encoder. The moving-coil actuator could be controlled by a program from a PC, operating with either a constant acceleration mode or a constant velocity mode. The velocity of the moving-coil-actuator is plotted as a functions of time for the constant acceleration mode and the constant velocity mode in Fig. 2a and b, respectively. In Fig. 2a, the acceleration was set at $\pm 10 \text{ mm/s}^2$, and then the velocity was changed in a range of $\pm 6 \text{ mm/s}$ with a duration of one cycle of 2.8 s. The average error of velocities for an ideal constant acceleration mode was 0.25 %. In Fig. 2b, on the other hand, the velocity was set at +10 and -5.42 mm/s with the duration of one cycle of 1.4 s. The average error of the velocity was 0.31 %. This value

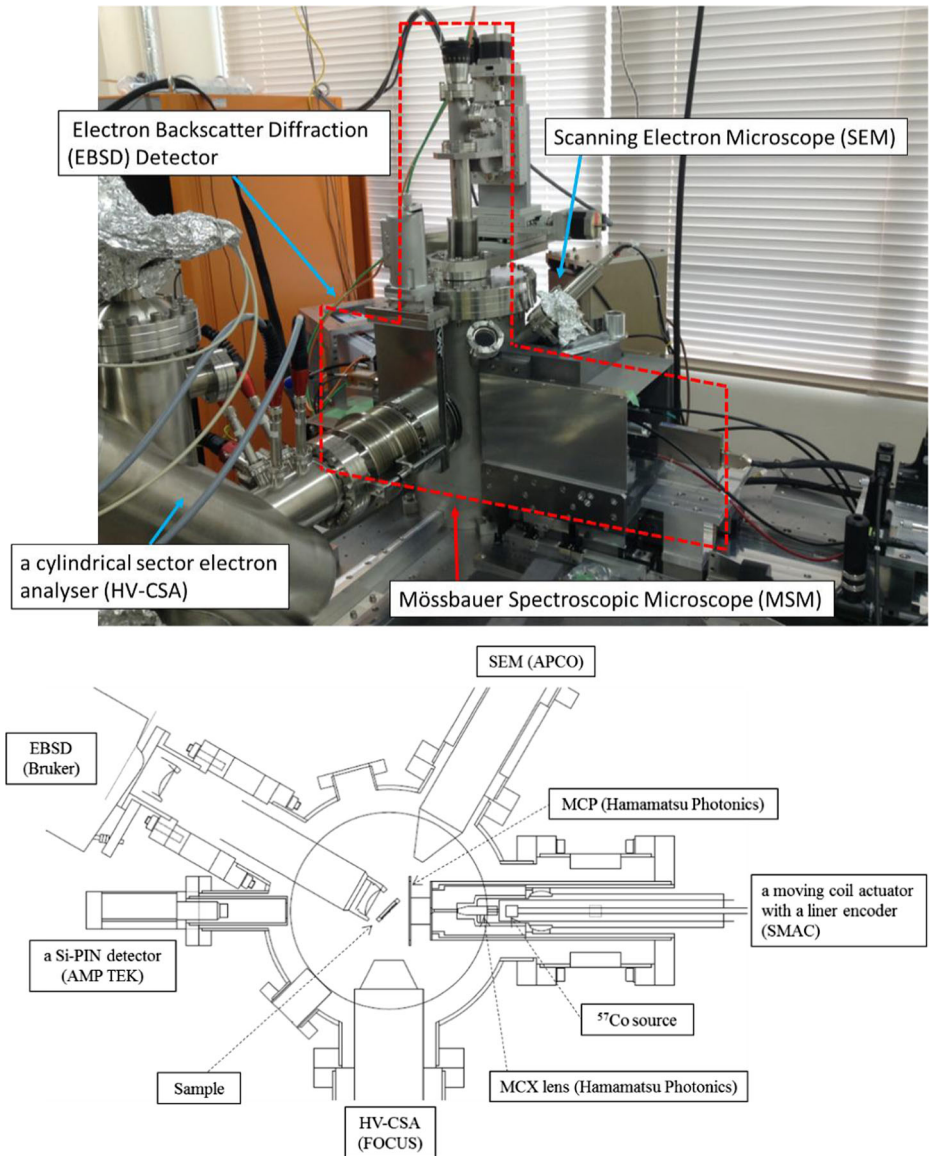


Fig. 1 Photograph and plan view of the 3D-Mössbauer spectroscopic microscope under development

corresponds to the error of 0.017 mm/s, appearing to be sufficiently small as compared to the line width.

Figure 2c presents the Mössbauer spectra of α -Fe foil with a thickness of 28 μm . The Mössbauer spectra were measured either by a conventional Mössbauer driver (the upper spectrum), or by the moving-coil actuator with the constant acceleration mode (the middle spectrum) and also the constant velocity mode (the lowest spectrum). The sharp sextet of α -Fe indicates that the moving-coil actuator can be used as a Mössbauer driver. In the case of the constant acceleration mode, however, the FWHMs of each line were 0.414,

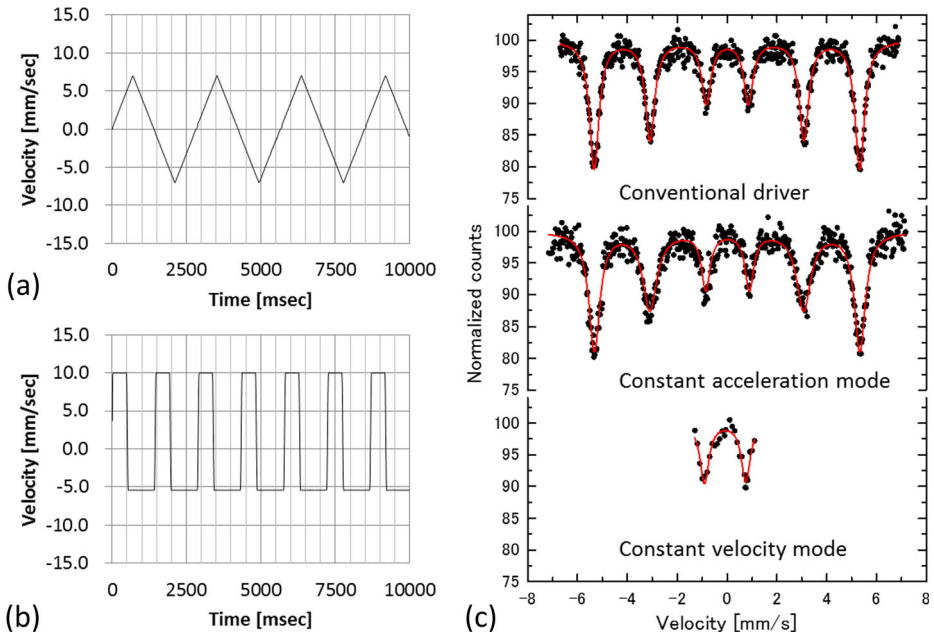


Fig. 2 Velocity of the moving-coil-actuator as functions of time with **a** the constant acceleration mode (acceleration = ± 10 mm/s²) and **b** the constant velocity mode (velocity = +10 and -5.42 mm/s), respectively. **c** The Mössbauer spectra were measured either by a conventional Mössbauer driver, or by the moving-coil actuator with the constant acceleration mode and also the constant velocity mode for α -Fe foil with a thickness of 28 μ m

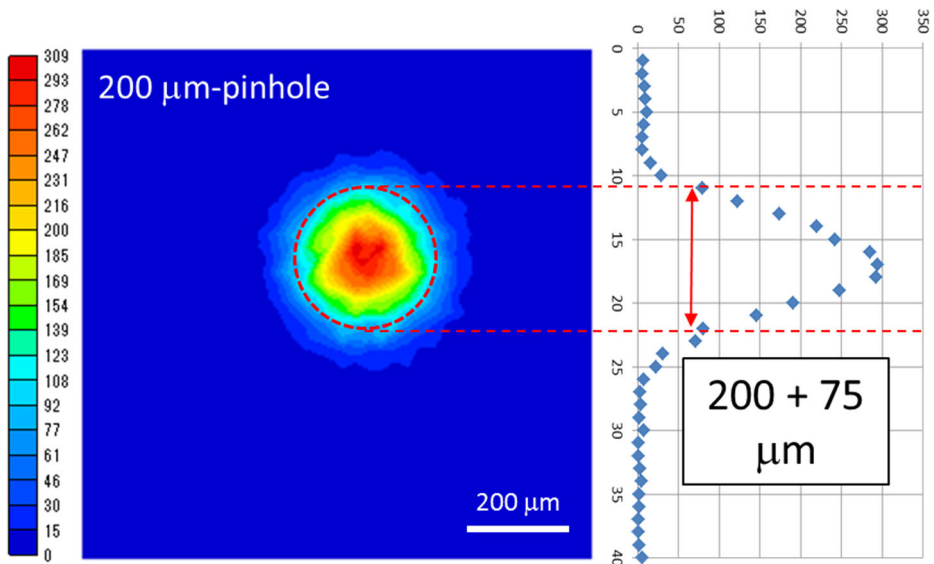


Fig. 3 Mapping image of a γ -rays spot focused with MCX lens. It also shows line profile through the spot center

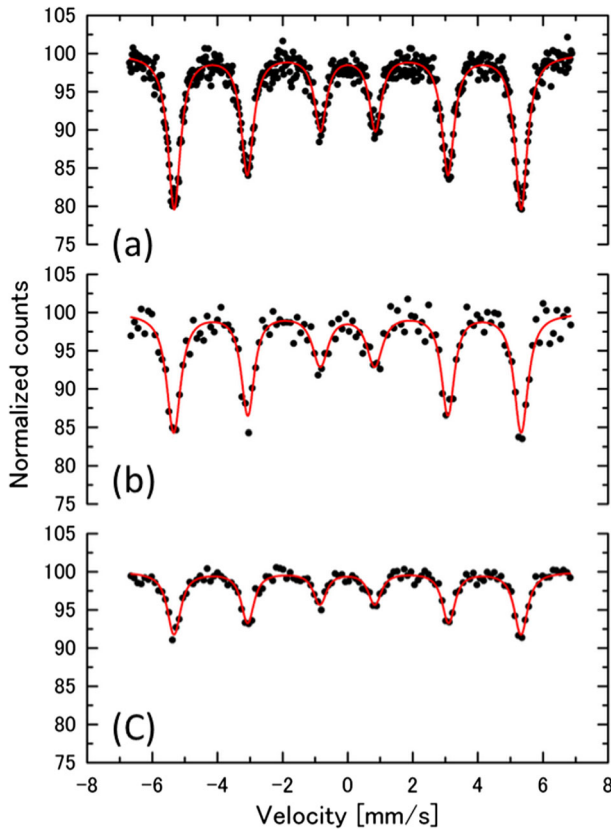


Fig. 4 Mössbauer spectra of 28 μm -thick $\alpha\text{-Fe}$ -foil **a** without MCX lens (γ -rays through a Pb collimator with a diameter of 2 mm ϕ), **b** with MCX lens (the spot size of 250 $\mu\text{m}\phi$ and the focus length 100 mm), and **c** with MCX lens (75 $\mu\text{m}\phi$ and 50 mm)

0.678, 0.532 mm/s from inside to outer peaks, respectively. The broad 2–5 lines suggest that the velocity control must be imperfect and further improved. In the case of the constant velocity mode, on the other hand, the FWHM of 3–4 lines was 0.435 mm/s. Therefore, the constant velocity mode appears to provide a precise control on the Doppler velocity, yielding a certain Mössbauer spectral component without a serious line broadening. This result makes us possible to use this actuator system for the mapping measurements on Fe impurities in mc-Si matrix.

The spot size of γ -rays focused with MCX lens is shown in Fig. 3. The image was obtained by mapping the transmitted 14.4 keV- γ -rays through a Ta-pinhole of 200 $\mu\text{m}\phi$ in diameter. It also shows the line profile through the spot center. The FWHM of the spot was about 275 μm , thus the spot size was estimated to be 75 $\mu\text{m}\phi$ in diameter. This value is small enough to distinguish the grains in mc-Si.

The Mössbauer spectra of a 28 μm -thick $\alpha\text{-Fe}$ -foil were measured with/without MCX lens. Figure 4a corresponds to the spectrum without MCX lens, i.e., γ -rays are passing through only a lead collimator with a diameter of 2 mm ϕ from ^{57}Co -in-Rh source. Figure 4b and c are the spectra with different MCX lens, respectively: The MCX lens used for Fig. 4b

Table 1 FWHMs and absorption areas of each spectrum in Fig. 4a–c

	FWHM [mm/s]			Absorption area [%]
	3–4 lines	2–5 lines	1–6 lines	
(a) without MCX lens	0.444	0.454	0.463	20.9
(b) with MCX lens (focus length 100 mm)	0.542	0.428	0.474	17.7
(c) with MCX lens (focus length 50 mm)	0.434	0.424	0.450	8.9

has a spot size of $250 \mu\text{m}\phi$ and a focal distance of 100 mm, while the lens for Fig. 4c provides the spot of $75 \mu\text{m}\phi$ and the focal distance of 50 mm. The FWHM and absorption areas of each spectrum in Fig. 4a–c are summarized in Table 1. The FWHMs of the spectra with both MCX lens are rather sharp as in the case without MCX lens. However, the absorption area with MCX lens decreases apparently than that without MCX lens. In particular, the absorption area in Fig. 4c decreases to the half of the area in Fig. 4a. As the γ -rays are focused with MCX using a total reflection on the inner walls of the micro-capillaries, the number of the total reflections must increase by reducing both the spot size and the focal distance. The reason for the smaller absorption areas appears to be due to a small energy loss of the γ -rays in the capillaries. Therefore, we are still optimizing the MCX lens presently by selecting the lens parameters, such as a focal distance, a spot size and an absorption area.

Figure 5a–e provide the images observed in a region of mc-Si solar cells, which are obtained by CMOS camera (a), SEM (b), EBIC (c), EBSD (d) and (e), respectively. The SEM image (b) shows a vertical bright band of Ag electrode at the right hand side, and an edge-shape grain at the left hand side, as is also seen in Fig. 5a. The EBIC image (c) contains the similar contrast corresponding to the SEM image. Since the EBIC image is formed due to the current flowing from the observed surface to the backside electrode, the contrast becomes dark at a place where a carrier recombination center exists such as an electrode, electrically active dislocations as well as grain boundaries. Indeed, this EBIC image yields a broader contrast at the Ag electrode than that of the SEM image, because the electron beam current flows into the Ag electrode also from the region near the electrode. Thus, a carrier recombination center in mc-Si samples can be detected by EBIC technique [5].

Figure 5d is an inverted pole figure map along a normal direction of EBSD for the area, which is indicated by the square in Fig. 5a. The crystal orientations are colored corresponding to the coloring shown in the unit triangle pole figure at the lower right hand side of the figure. There is a good correlation between the EBSD and the EBIC images. The structures of grain boundaries are identified from the orientation of each grain: there are twin boundaries of $\Sigma 3$, coincidence boundaries of high Σ such as $\Sigma 35\text{a}$, and random boundaries of R. Figure 5e is a local misorientation map depicted analytically from the change in orientation at each mapping point, which is corresponding to residual strains. This mapping image indicates that there exist large strain distributions in the grain as well as near the electrode.

Figure 6 show (a) CMOS photograph and (b), (c) and (d) MSM images for an area of the mc-Si solar cell. The rectangular region in Fig. 6a is measured by SEM, EBIC and EBSD, as presented in Fig. 5. The MSM images of (b) and (c) are obtained by the transmitted

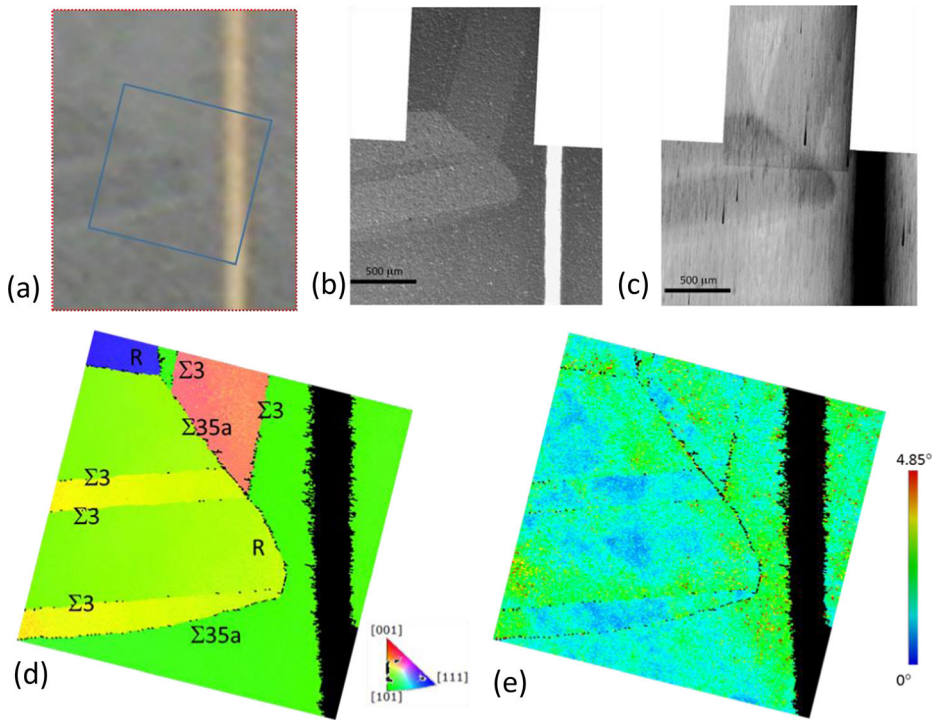


Fig. 5 Images correspond to the region including same grains in mc-Si solar cells, which are observed by CMOS camera (a), SEM (b), EBIC (c), inversed pole figure map of EBSD (d), and local misorientation map by EBSD (e)

14.4-keV- γ -rays and by the emitted electrons, respectively. The MSM was operated with a constant velocity mode corresponding to the peak position of a neutral interstitial Fe_{int}^0 [1–4]. The spot size of MCX lens used in the mapping was $250 \mu\text{m}\phi$. In the γ -rays image (b), on one hand, Ag electrodes with a width of $100 \mu\text{m}$ can be clearly seen at the center as well as at the most left hand side, although the overall γ -rays intensity appears to distribute rather homogeneously. This indicates that the MCX lens has the spatial resolution smaller than $100 \mu\text{m}$. In the electron images (c), on the other hand, the electron intensity changes strongly in the different grains.

Figure 6d is a superposition of the electron mapping (c) and the photograph (a). The grain boundaries are drawn into the image based on Fig. 6a. Higher electron intensities are observed both at the upper and lower right regions and at the lower left regions, corresponding to different grains of the mc-Si solar cell. The result suggests that a considerable amount of Fe impurities up to 10^{16}cm^{-3} are incorporated through the production processes, i.e., from the feedstock as well as from the mold release agent of the crucible wall during melting [6].

Presently, we are trying to realize a 3D-mapping technique by combining the 2D-mapping technique and a depth-selective electron measurement using an electron spectrometer, HV-CSA [7]. Conversion and Auger electrons are emitted from the Fe nuclei excited

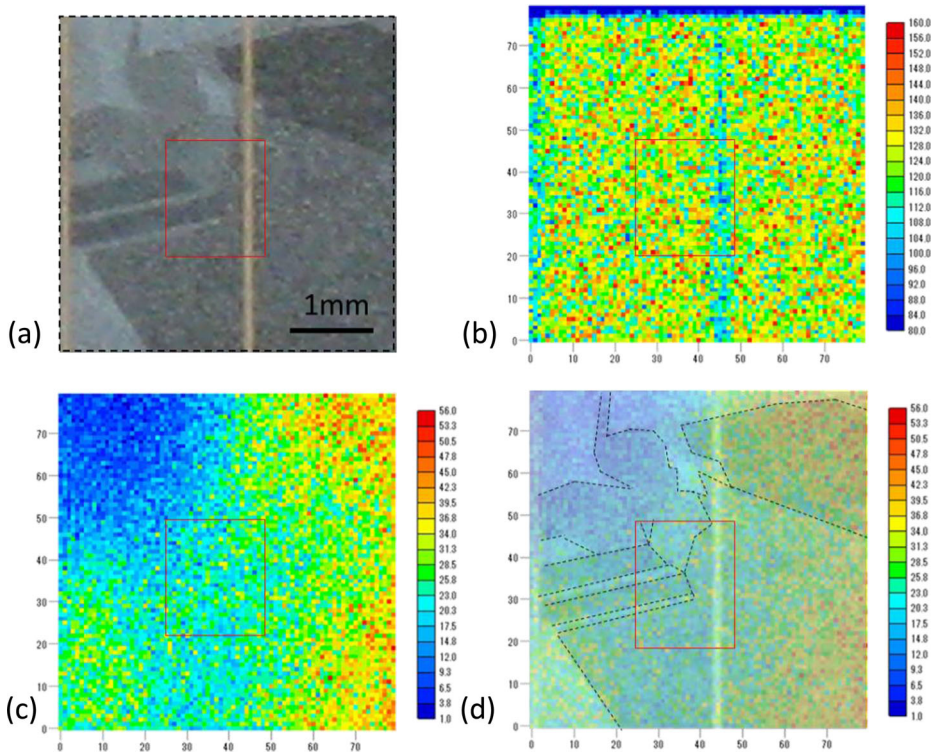


Fig. 6 **a** CMOS photograph, **b** and **c** MSM images centered in the region of Fig. 5: **b** a transmitted 14.4-keV- γ -rays map, **c** MCP signals map. **d** A superposition of the MCP signal map and the photograph

by resonance absorption of γ -rays, and lose the energy due to inelastic scattering until they arrive the surface. Therefore, it is possible to obtain a depth distribution of Fe atoms by a precise measurement of the energy loss for conversion and Auger electrons. This technique is called depth selective conversion Mössbauer spectroscopy (DSCEMS), has the detection limit of 10^{14} atoms/cm², the probing depth of about 100 nm, and the depth resolution of 5–10 nm for ^{57}Fe [8]. Previously, we measured the electron intensity by a MCP detector emitted from a Si wafer which was deposited by Ag layers with different thicknesses of 20, 50, 70 nm on a ^{57}Fe layer. Successfully we detected different electron intensities depending on the Ag layer thickness [9]. This results indicates that we can obtain a depth profile for ^{57}Fe in a depth of 100 nm with the resolution of 20 nm.

In order to test the energy resolution of HV-CSA equipped with MSM, we measure elastic scattering peak of electron beams of SEM. The result is shown in Fig. 7. Electron beams are scattered elastically on a Fe foil, and then the kinetic energy is measured by HV-CSA (the electrons are decelerated to 100 eV and pass through the analyzer). Since the dispersion of electron energy with an electron gun is sufficiently small, the broadening of the peak width is caused by the analyzer. Under a typical condition, FWHM of the peak of elastic scattered electrons was 1.8–2.2 eV. These values must be sufficient to measure the energy loss for conversion and Auger electrons in order to obtain a depth profile.

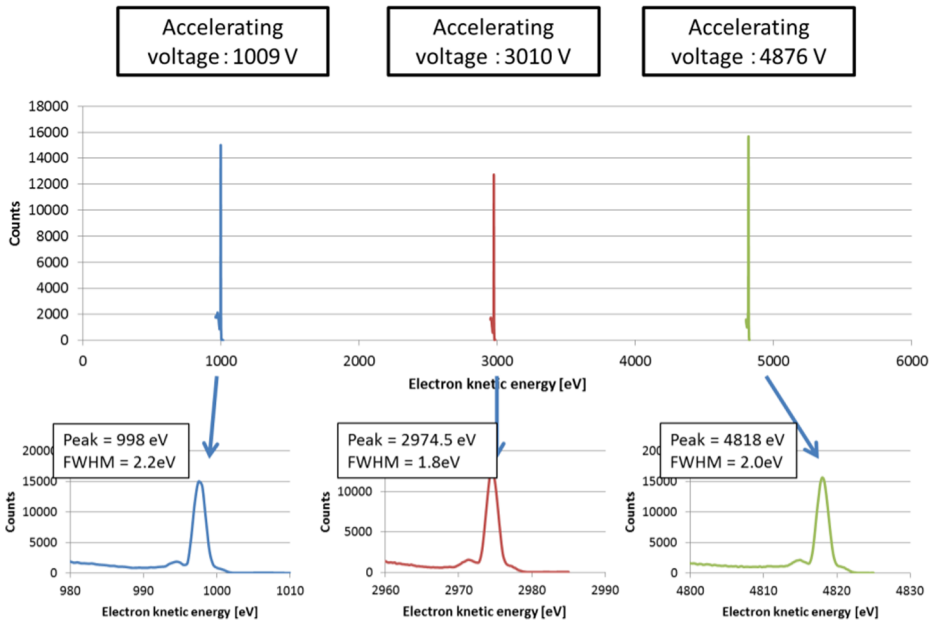


Fig. 7 Result of the test operation of HV-CSA equipped with MSM for elastic scattered electrons

4 Summary

The new MSM is constructed using a new moving-coil linear-actuator, a newly de-signed multi-capillary X-ray (MCX) lens, and a funnel-type micro channel plate (MCP) detector. The new system provides a precise Doppler velocity control both for a constant velocity and a constant acceleration operations, also a smaller spot size of the focused γ -rays, and a better detection efficiency for the electrons than those of the former MSM [1]. Furthermore, we present the typical observations obtained by this newly constructed set-up. The SEM and the EBIC observations show the grain structure and the distribution of residual strains in a mc-Si solar cell, and in addition the EBIC images clarify the regions where the electro-active defects exist. In the same area, we perform the MSM mappings by selecting the constant Doppler velocity which corresponds to the neutral interstitial Fe_{int}^0 component with the isomer shift of +0.40 mm/s [3]. Accordingly, it is possible for us to measure the mapping image only due to the interstitial Fe_{int}^0 distributing in the grains of a mc-Si solar cell.

Acknowledgments This work is supported by “Development of Systems and Technologies for Advanced Measurement and Analysis” Program of Japan Science and Technology Agency (JST). We are grateful to Dr. Hiroshi Kubo for helpful discussions.

References

1. Yoshida, Y., Suzuki, K., Hayakawa, K., Yukihiro, K., Soejima, H.: *Hyperfine Interact.* **188**, 121 (2009)
2. Hayakawa, K., Akiyama, Y., Tsukamoto, Y., Kurata, M., Yukihiro, K., Soejima, H., Yoshida, Y.: *Hyperfine Interact.* **206**, 79 (2012)
3. Yoshida, Y., Tsukamoto, Y., Ichino, M., Tanaka, K.: *Solid State Phenom.* **40**, 205–206 (2013)

4. Tanaka, K., Akiyama, Y., Hayakawa, K., Yukihiro, K., Yoshida, Y.: *Hyperfine Interact.* **206**, 75 (2012)
5. Chen, J., Sekiguchi, T., Xie, R., Ahmet, P., Chikyo, T., Yang, D., Ito, S., Yin, F.: *Scripta Mater.* **52**, 1211 (2005)
6. Macdonald, D., Cuevas, A., Kinomura, A., Nakano, Y., Geerligs, L.J.: *J Appl. Phys.* **97**, 033523 (2005)
7. Rubio-Zuazo, J.R., Escher, M., Merkel, M., Castro, G.R.: *J. Phys.: Conf. Ser.* **100**, 072032 (2008)
8. Sawicki, J.A.: In: Long, G.J., Stevens, J. (eds.) *Industrial Applications of the Mössbauer Effect*, pp. 83–120. Plenum Press, New York and London (1986)
9. Yoshida, Y.: Japan Patent 129585 (2007)